Short Papers

A Robot Finger Design Using a Dual-Mode Twisting Mechanism to Achieve High-Speed Motion and Large Grasping Force

Young June Shin, Ho Ju Lee, Kyung-Soo Kim , *Member, IEEE*, and Soohyun Kim

***Abstract*—A dual-mode robot finger is proposed to achieve a high-speed motion and large grasping force with a single motor. The robot finger has two actuator modes, which consist of the speed mode and the force mode. Based on the geometric analysis of each mode, the main design parameters of the proposed robot finger are derived, and their effectiveness is verified by simulations. In addition, using experiments with a prototype of a robot finger, the validity of the proposed approach is demonstrated.**

***Index Terms*—Dual-mode robot finger, fast bending motion, grasping force, twisted string actuation.**

I. Introduction

The development of anthropomorphic robot hands is one of the major issues in the field of robotics. A large number of research studies have been devoted to implementation of the typical functions and shapes of human hands [1]–[4]. However, the field is still far from replicating the generic features of human hands such as delicacy and dexterity of finger manipulation, relatively fast motion, and high grasping force with thin and light structures.

To improve performance, various types of actuators have been adopted for the design of robot hands such as shape memory alloy wires [5], [6], ultrasonic motors [7], pneumatic actuators [8], [9], and electroactive polymer actuators [10]. These actuators may satisfy some, but not all of the features in terms of the speed, output (grasping) force, and the weight (or volume). Additionally, an improvement of the electromagnetic motors has been achieved by reducing the size but enhancing the output torque [11]. It should be noted, however, that motors with gears inevitably result in a heavy robot hand.

In parallel, to compensate for the weakness of actuators, attempts have been made to devise more optimized mechanisms that provide the functionalities of human hands. One of the representative approaches is to use underactuated mechanisms, as in [12] and [13]. This provides a larger degree of freedom in finger operations with a small number of actuators. However, in general, this type of mechanism decreases the dexterity. More recently, to achieve high-speed motion and large grasping force, power transmission mechanisms have been proposed in the literature [14]–[16]. These approaches are quite satisfactory in terms of the performance, but they have been criticized for bulky size and the number of actuators required.

Manuscript received January 6, 2012; revised May 29, 2012; accepted June 25, 2012. Date of publication July 24, 2012; date of current version December 3, 2012. This paper was recommended for publication by Associate Editor T. Murphey and Editor W. K. Chung upon evaluation of the reviewers' comments. This work was supported by the Unmanned Technology Research Center, Korea Advanced Institute of Science and Technology, originally funded by the Defense Acquisition Program Administration, Agency for Defense Development.

The authors are with the Department of Mechanical Engineering, Korea Advanced Institute of Science and Technology, Daejeon 305-701, Korea (e-mail: yjsin@kaist.ac.kr; bluesunset@kaist.ac.kr; kyungsookim@kaist.ac.kr; soohyun@kaist.ac.kr).

Color versions of one or more of the figures in this paper are available online at http://ieeexplore.ieee.org.

Digital Object Identifier 10.1109/TRO.2012.2206870

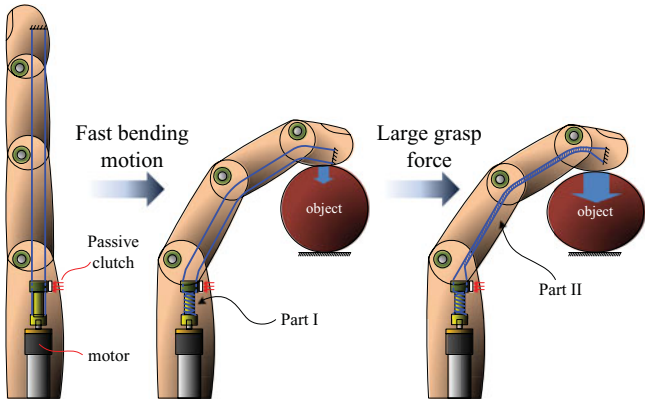

Fig. 1. Concept of a dual-mode robot finger.

Despite many approaches, designing a light-weight and high-speed robot hand with large grasping force is still an unsolved problem. Motivated by the design challenge, this paper is devoted to proposing a design in which speedy motion and large grasping forces are both available, depending on the operational modes. For instance, the output force of a robot finger may not be necessarily large when it moves fast. The robot finger could move slowly if large force is needed. To implement this idea, we propose a new type of power transmission, referred to as *dual-mode* actuation, by combining the twisted string actuation method described in [17] and [18] with a passive clutch mechanism. When the reaction at the fingertip is small, the finger moves at a high speed. However, the fingertip force (i.e., grasping force) may gradually increase as the finger slows down due to the reaction from the environment. To propose the design guidelines, the design parameters are derived analytically. Based on these results, a prototype of the robot finger is developed. Through experiments, the effectiveness of the proposed method is demonstrated.

This paper is organized as follows. In Section II, a concept for a dual-mode robot finger is introduced. Section III is devoted to the analysis of the proposed robot finger and fingertip force and the numerical simulation. Section IV describes the actual implementation of a dual-mode robot finger. In Section V, the experiments with the developed robot finger are presented. Finally, the conclusion follows in Section VI.

II. Dual-Mode Robot Finger

Suppose that an electromagnetic motor has a power P, a rotation speed $\dot{\theta}$, and a torque τ_m. Then, considering that $P = \tau_m \dot{\theta}$, given a power, the motor can generate a high-speed rotation if the torque is small. The converse is also true. Inspired by this fact, we suggest a dual-mode robot finger utilizing double-twisted string mechanisms, as shown in Fig. 1. Observe that the robot finger moves fast until it reaches the object, as the strings are quickly wound in Part I. Then, as the reaction force from the object increases, the strings in Part II begin to be wound and contract, which eventually increases the grasping force. The mechanical structure is very simple to implement as shown in Fig. 2. The mechanism consists of two twisting couplings labeled TC1 and TC2, a shaft between them, two strings, and a brake. TC1 is fixed at the motor axis so that the rotation of TC1 is synchronized with the motor. In addition, the strings coming through the holes of TC2 are

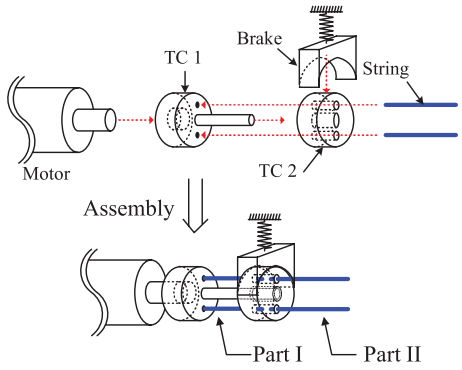

Fig. 2. Mechanical structure of the dual-mode actuation.

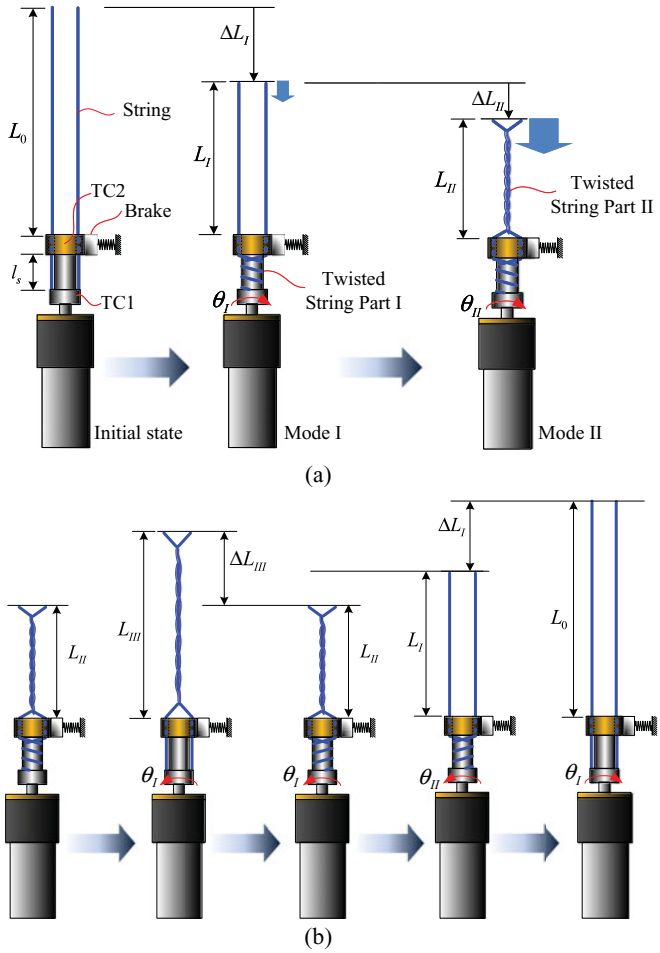

Fig. 3. Driving concept of the dual-mode twisting mechanism. (a) Contraction process. (b) Relaxation process.

fixed at the right-hand surface of TC1. Note that TC2 can rotate around a shaft fixed at TC1 when the torque transmitted by the twisted strings around the shaft (between TC1 and TC2) exceeds the friction imposed by the brake. If TC2 rotates, the strings in Part II would be twisted with a small radius.

The contraction principle of the dual-mode mechanism is demonstrated in Fig. 3(a). When the motor axis (together with TC1) starts the rotation, the strings are twisted on the shaft until the fingertip reaches the object. However, TC2 may not rotate because of the friction imposed by the brake. This operational mode is called Mode I (which implies the *speed* mode).

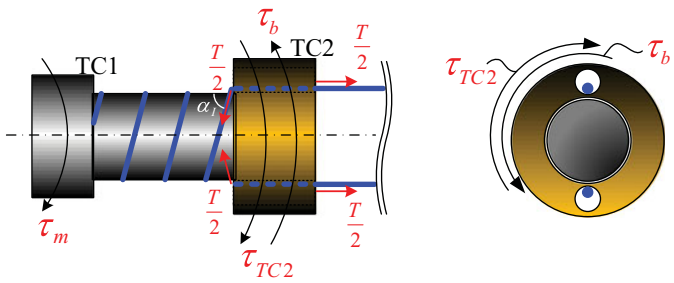

Fig. 4. Free-body diagram of the twisting mechanism.

Suppose that a sufficiently large tension force T is applied to the string as shown in Fig. 4 (e.g., the robot finger contacts the object). Then, under the assumption that the friction on the hole in TC2 can be negligible, one may have from [17]

$$T = \frac{\tau_m}{R_t \sin \alpha_I} \tag{1}$$

where α_I is a helical slope, and τ_m is the motor torque. Hence, the transmitted torque to TC2 is as follows:

$$\tau_{TC2} = R_t T \sin \alpha_I = \tau_m . \tag{2}$$

This implies that TC2 rotates if

$$\tau_m > \tau_b \tag{3}$$

where τ_b is the frictional torque by the brake. In the end, two strings in Part II are twisted, which produces a high contracting force, while the speed of contraction gets much slower. This mode is called Mode II (which implies the *high-force* mode).

Now, let us consider the relaxation procedure shown in Fig. 3(b). Assume that one end of the strings is tightly pulled by the reaction force (e.g., by torsional springs of each joint in the robot finger). The twisted strings in Part I would be unwound when the motor rotates reversely. To unwind the twisted strings in Part II, a larger torque than the braking torque should be transmitted to TC2. Then, TC2 starts rotating to unwind the twisted strings in Part II. Finally, it returns to the initial state by unwinding the twisted string in Part I.

It is noted that, due to the passive operation of the brake on TC2, the robot finger behaves twitched during the relaxing process, which is a drawback of the proposed mechanism. It is expected that this will be solved by adopting an active brake in order to determine the locking and releasing moments for mode changes. This remains as an important future study.

The twisted string actuation method was originally proposed in [19]. By simply twisting two or more strings, a large contracting force can be generated without mechanical gears. Nevertheless, the method in [19] has a generic disadvantage in the slow contraction speed. However, the proposed approach provides a solution to the issue by utilizing the dual-mode concept.

III. Analysis of the Dual-Mode Robot Finger

In this section, the bending speed and fingertip force of a dual-mode robot finger are considered to derive the main design parameters. Then, based on the numerical analysis, a design guideline is provided to specifically determine the design parameters.

A. Contraction Length for Bending Motion

First, let us consider the contraction length of the strings in each mode. As shown in Figs. 3 and 5, the twisted strings with a helical

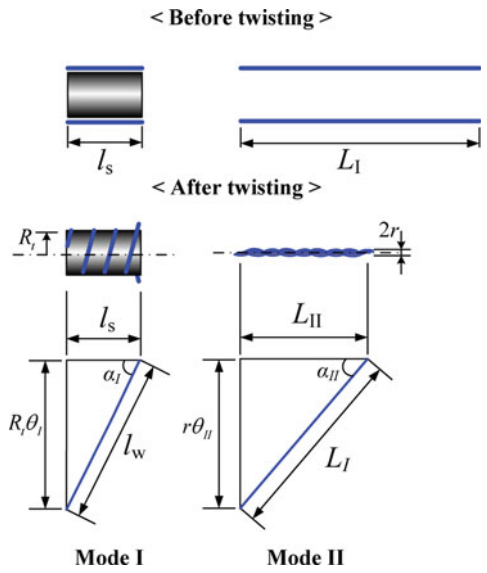

Fig. 5. Representation of the twisted strings for both modes.

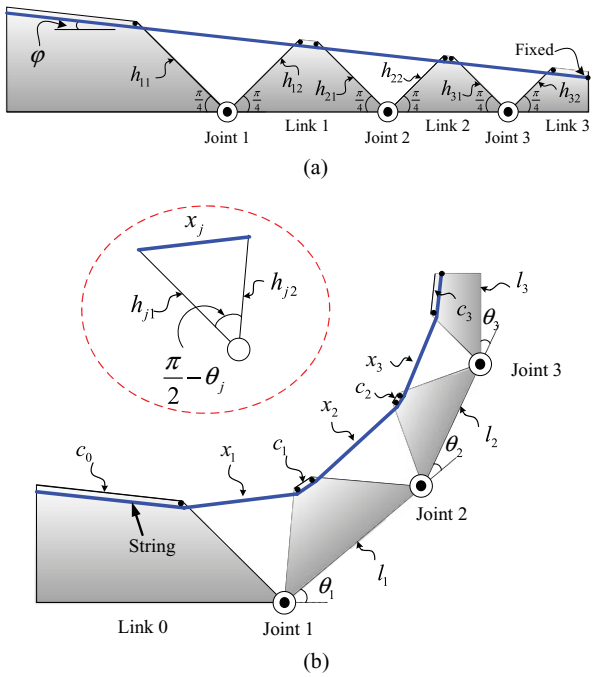

Fig. 6. Schematic diagram of the robot finger. (a) Bending posture. (b) Fully extended posture.

shape for each mode can be treated as the hypotenuse of a triangle. Then, the contractions of the twisted strings are as follows:

$$\begin{cases} \Delta L_I = l_w - l_s = \sqrt{(R\theta_I)^2 + l_s^2} - l_s, & \text{for Mode I} \\ \Delta L_{II} = L_I - L_{II} = L_I - \sqrt{L_I^2 - (r\theta_{II})^2}, & \text{for Mode II} \end{cases} \tag{4}$$

where θ_I and θ_{II} are the rotation angles of the motor in Mode I and Mode II, respectively, and R and r are the radii of the shaft and string, respectively. Note that the length of the shaft l_s and the length of the untwisted strings in Part II (L_I) are all fixed.

Second, suppose that the robot finger is designed as shown in Fig. 6.

The length of the strings is geometrically determined depending on the posture of the robot finger. That is, for a bending posture of the robot finger, it is noted that the length of string between links j and $j-1$ at joint j is as follows:

$$x_j = \sqrt{h_{j1}^2 + h_{j2}^2 - 2h_{j1}h_{j2}\sin\theta_j} \tag{5}$$

where θ_j is the joint angle at joint j.

From Fig. 6(b), the total length of string required for a fully extended posture is easily determined by

$$X_o = \sum_{j=1}^{3} x_{oj} + \sum_{k=0}^{3} c_k \tag{6}$$

where $x_{oj} \triangleq \sqrt{h_{j1}^2 + h_{j2}^2}$ and c_k are the constants determined by the geometry of the robot finger.

To achieve the bending posture in Fig. 6(a), from the fully extended posture in Fig. 6(b), the string should be contracted as much

$$\begin{aligned} \Delta X &= X_o - X = \Delta x_1 + \Delta x_2 + \Delta x_3 \\ &= \sum_{j=1}^{3} \sqrt{h_{j1}^2 + h_{j2}^2} - \sum_{k=1}^{3} \sqrt{h_{k1}^2 + h_{k2}^2 - 2h_{k1}h_{k2}\sin\theta_k} \end{aligned} \tag{7}$$

where $\Delta x_j = x_{oj} - x_j$ for $j = 1, 2, 3$.

Now, to compare the bending speed, let us derive the rotation angles of the motor required to achieve the same contraction length of the string in the following.

For Mode I, from $\Delta L_I = \Delta X$

$$\theta_{\text{req},I} = \frac{1}{R}\left\{\left(l_s + \sum_{j=1}^{3}\sqrt{h_{j1}^2 + h_{j2}^2} - \sum_{k=1}^{3}\sqrt{h_{k1}^2 + h_{k2}^2 - 2h_{k1}h_{k2}\sin\theta_k}\right)^2 - l_s^2\right\}^{\frac{1}{2}}. \tag{8}$$

For Mode II, from $\Delta L_{II} = \Delta X$ and $L_I = L_o$

$$\theta_{\text{req}.II} = \frac{1}{r}\left\{L_o^2 - \left(L_o - \sum_{j=1}^{3}\sqrt{h_{j1}^2 + h_{j2}^2} + \sum_{k=1}^{3}\sqrt{h_{k1}^2 + h_{k2}^2 - 2h_{k1}h_{k2}\sin\theta_k}\right)^2\right\}^{\frac{1}{2}}. \tag{9}$$

Note that, to reach a target posture from a fully extended posture, the rotational angle of the motor in Mode I should be much smaller than that of Mode II because of $R \gg r$. This implies that the contraction speed in Mode I is much faster than that of Mode II. Generally, R and r are the major parameters for making a difference in the bending speed.

B. Derivation of Fingertip Force

To derive the fingertip force, a force diagram of each joint is considered, as shown in Fig. 7. The torques exerted at each joint are generated by the contraction force of the strings. One may derive the generated torques, $\tau = [\tau_1, \tau_2, \tau_3]^T \in \mathbb{T}_{\text{all}}$, as follows:

$$\begin{aligned} \tau_1 &= Th_{12}\sin\psi_{12} - (T - f_1)\,h_{21}\sin\psi_{21} - k_1\theta_1 \\ \tau_2 &= (T - f_1)\,h_{22}\sin\psi_{22} - (T - f_1 - f_2)\,h_{31}\sin\psi_{31} - k_2\theta_2 \\ \tau_3 &= (T - f_1 - f_2)\,h_{32}\sin\psi_{32} - k_3\theta_3 \end{aligned} \tag{10}$$

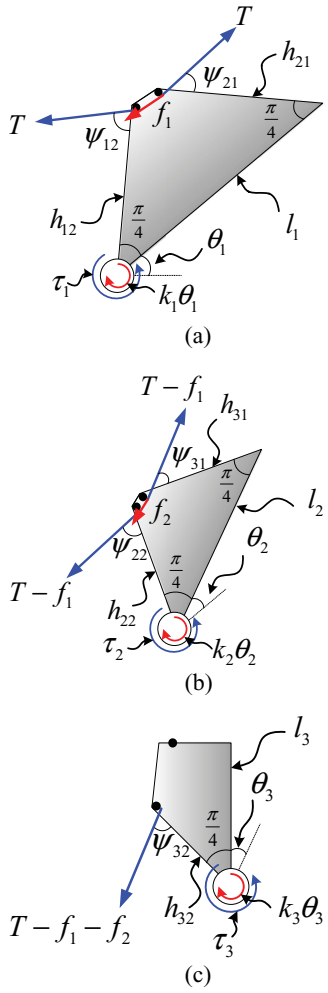

Fig. 7. Free-body diagram of each link. (a) Link 3. (b) Link 2. (c) Link 1.

where $\mathbb{T}_{\text{all}}$ is the set of allowable torque vectors, T is the contraction force, k_j is the stiffness coefficient of the torsional spring for $j = 1, 2, 3$, and f_1 and f_2 are the Coulomb friction between the string and link, which are given by

$$\begin{cases} f_1 = \mu_1 T \left\{ \sin\left(\psi_{12} - \dfrac{\pi}{4} + \varphi\right) + \sin\left(\psi_{21} - \dfrac{\pi}{4} + \varphi\right) \right\} \\ f_2 = \mu_2 \left(T - f_1\right) \left\{ \sin\left(\psi_{22} - \dfrac{\pi}{4} + \varphi\right) + \sin\left(\psi_{31} - \dfrac{\pi}{4} + \varphi\right) \right\} \end{cases} \tag{11}$$

where μ_1 and μ_2 are the frictional coefficients, and φ is a geometric slope of the robot finger as shown in Fig. 6(b). Here, based on the analysis in [17], the contraction force T generated by twisting the string in the robot finger is obtained for each mode as follows:

$$T = \begin{cases} \dfrac{\tau_m}{R_t \sin \alpha_I}, & \text{for Mode I} \\ \dfrac{\tau_m - \tau_b - \tau_f}{r \tan \alpha_{II}}, & \text{for Mode II} \end{cases} \tag{12}$$

where $R_t = R + r$, α_I and α_{II} are the helical slopes, τ_m is the motor torque, and τ_b and τ_f are the braking torques exerted on TC2 and the frictional loss torque between the string and the structure, respectively. Then, the fingertip force can be described by

$$F = (JJ^T)^{-1} J\tau^* \tag{13}$$

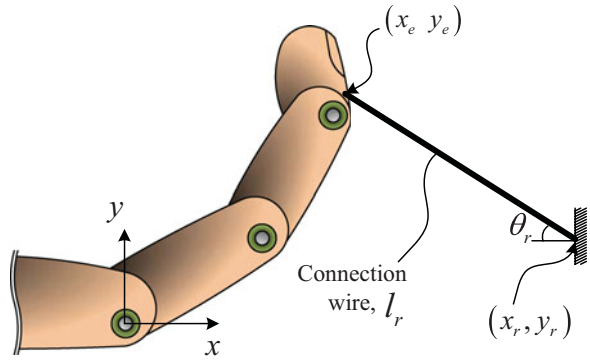

Fig. 8. Constraint for a numerical analysis of the robot finger.

TABLE I
SIMULATION PARAMETERS

Items	Specifications
Link(mm)	$l_1 = 45$, $l_2 = 25$, $l_3 = 15$
Shaft Length(mm)	$l_s = 12$
Length of the strings(mm)	$L_o = 83$
Length of h_{j1}(mm)	$h_{11} = 12.4$, $h_{21} = 8.2$, $h_{31} = 5.9$
Length of h_{j2}(mm)	$h_{12} = 10.9$, $h_{22} = 7.3$, $h_{32} = 5.2$
Position of wire, (x_r, y_r)	(135 mm,-36.2 mm)
Length of l_r(mm)	130
Stiffness coefficient(Nm/rad)	$k_1 = 0.01$, $k_2 = 0.01$, $k_3 = 0.01$
Friction coefficient	$\mu_1 = 0.2$, $\mu_2 = 1.0$
Motor torque(Nm)	$\tau_m = 0.02$
frictional torque(Nm)	$\tau_b = 0.0$, $\tau_f = 0.009$

where $J \in \mathbb{R}^{2\times 3}$ is the Jacobian matrix [1], and $\tau* \in \mathbb{T}^*$ is given, from [20], by

$$\mathbb{T}^* = \mathbb{T}_{\text{all}} \cap \text{Range}(J^T).$$

Note that F is a function of τ^*, which consequently implies that together with (10)–(12)

$$F \triangleq \begin{cases} F_I, & \text{for Mode I} \\ F_{II}, & \text{for Mode II} \end{cases} \tag{14}$$

Note that R and r dominantly affect the fingertip force. Overall, based on (8), (9), and (14), it turns out that the radii of the shaft and string are the major design parameters for the proposed mechanism.

C. Consideration of Design Parameters

Under the constraint that the robot finger is connected to a connection wire, as shown in Fig. 8, we performed a numerical analysis for two design parameters R and r, with the parameters summarized in Table I to develop the design guidelines of the proposed mechanism. Note that the quantities are obtained not arbitrarily but by actual measurements of the developed robot finger.

To investigate the bending motion speed and the fingertip force for each mode of the proposed robot finger, let us define the quantities as follows:

$$\alpha \triangleq \frac{\theta_{\text{req},II}}{\theta_{\text{req},I}} \tag{15}$$

$$\beta \triangleq \frac{|F_{II}|}{|F_I|}. \tag{16}$$

For all the pairs of $(R, r) \in$ [0.5 mm, 2 mm] $\times$ [0.1 mm, 0.5 mm], α and β are computed and plotted as shown in Figs. 9 and 10. Observe that α and β increase as does the ratio of R/r in general. This naturally

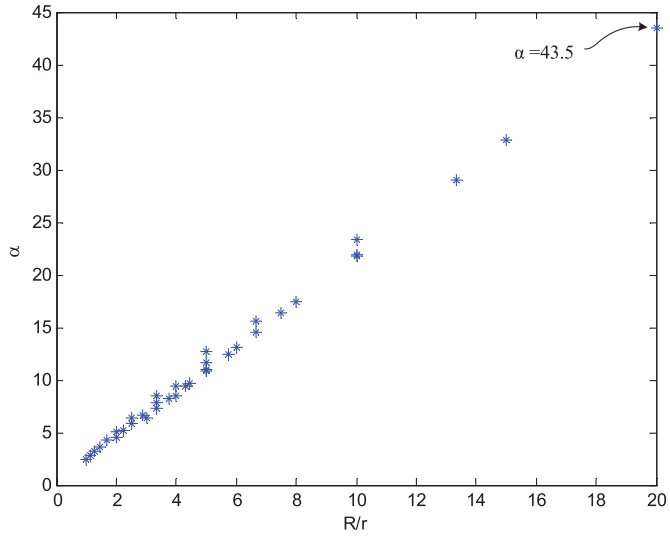

Fig. 9. Ratio of the required motor rotation angles depending on string contraction.

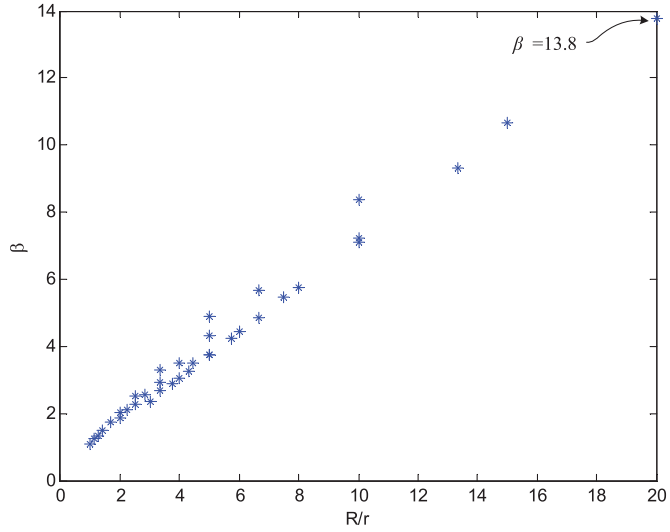

Fig. 10. Ratio of the fingertip forces for each mode.

shows that a dual-mode robot finger with fast motion and large grasping force can be achieved through a single motor if the radius of the shaft is large and that of the string is small. For instance, for $R = 2$ mm and $r = 0.1$ mm, which gives $R/r = 20$, the robot finger can move 43.5 times faster in Mode I than in Mode II, and generate a grasping force 13.8 times larger in Mode II than in Mode I.

In summary, designing the robot finger with a large value of R/r is desirable. However, there exist practical considerations, which limit R/r with a bound as follows.

1) The radius of the shaft R cannot be arbitrarily large. Since, in Mode I, $T = \frac{\tau}{R_t \sin \alpha_I}$ [i.e., (1)], the reaction force to bear by the robot finger in Mode I would be very small if R is too large. This means that Mode II would be easily activated under a small external load. Therefore, thus, the fast motion may not be achieved.
2) The radius of the string r should not be arbitrarily small to avoid the damage due to the stress induced by twisting.

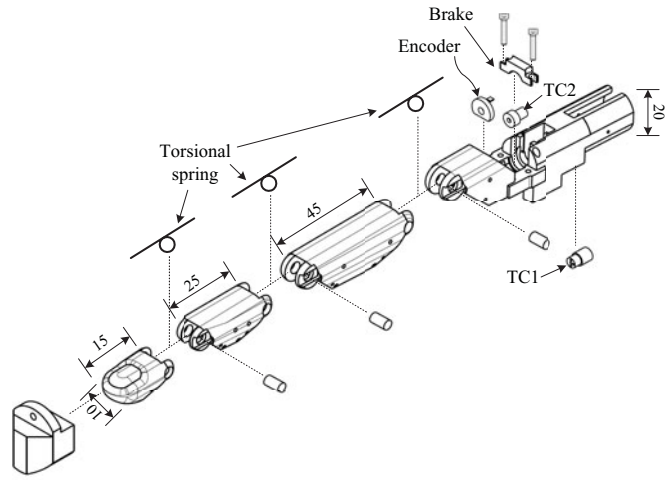

Fig. 11. Mechanical drawing of a dual-mode robot finger.

IV. Demonstration of the Dual-Mode Robot Finger

A. Design and Implementation

Based on the design considerations described in the previous section, we designed and implemented a dual-mode robot finger. For easy exposition, the mechanical drawing of the dual-mode robot finger is shown in Fig. 11. The robot finger consists of four links with three joints. For extension of the robot finger, torsional springs are embedded at each joint. The resistive encoders are embedded at each joint to control and measure the posture of the robot finger, and the magnetic encoder is also implemented in front of TC2 to measure the rotation of TC2. The motor, which uses a 1/16 reduction gear (Maxon motor 256101, ϕ 10, Switzerland) is located at Link 0, as shown in Fig. 12. To control the motor torque, a current sensor (WCS1702, Winson Semiconductor Corporation, Hsinchu, Taiwan) is implemented. The range of the joint angles is between 0° and 90°. Note that the size of the proposed robot finger is designed similarly to that of a standard human finger. The major specifications are summarized in Table II.

B. Operation of the Proposed Robot Finger

To verify the validity of the developed robot finger, we demonstrate the operation of the finger in Fig. 13. At first, bending and extending motions are repeated twice [see Fig. 13 (a)–(e)]. The robot finger is then bent more to exert a force on the load cell (BCL1kgf, CAS Corporation, East Rutherford, NJ) by tightly pulling the connection wire [see Fig. 13(f)–(j)]. Fig. 14 shows the measured results for the contracted length of string, rotation of TC2, the motor current, and the fingertip force. When there is no external load, the developed robot finger operates very quickly, in Mode I. When an external load is applied to the robot finger, the torque exerted on TC2 increases, and, finally, the robot finger generates a large fingertip force, in Mode II.

V. Experiments

A. Performance Measurements

To verify the effectiveness of the dual-mode robot finger, we measured the bending motion and fingertip force of the developed robot finger with the experimental setup shown in Fig. 15. To compare speeds and fingertip forces at each mode, we devised four cases as summarized in Table III. Note that the frictional force exerted on TC2 was properly

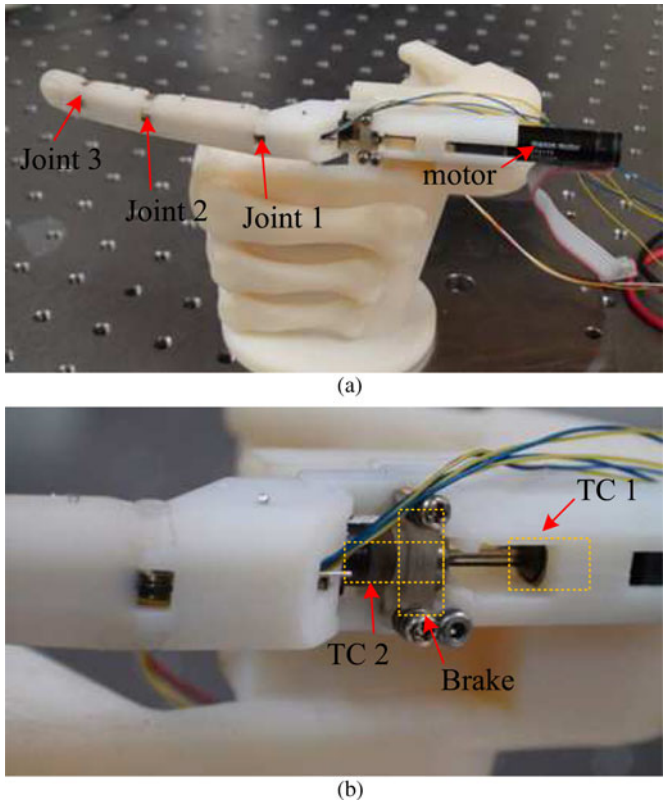

Fig. 12. Developed dual-mode robot finger. (a) Overall shape of the dual-mode robot finger. (b) Dual-mode twisting mechanism in the dual-mode robot finger.

TABLE II
SPECIFICATIONS OF THE PROPOSED ROBOT FINGER

Items	Specifications
Size (mm)	12(H) × 20(W) × 85(L)
Weight	29.9 g
Actuator	DC motor with 1/16 reduction gear (Maxon motor 256101, ϕ10)
Position sensor	Resistive-type encoder
Current sensor	WCS1702(Winson Semiconductor Corp.)
Joint angle range	$0 \leq \theta_j \leq 90^\circ$
Radius of shaft	$R = 0.5$ mm
Radius of string	$r = 0.1$ mm

adjusted so that the robot finger only operated in one mode for each case.

In Experiment 1, we measured the contraction speed of the strings for a given target fingertip position. To provide a constant rotation velocity for the motor in the finger, a proportional-integral-differential (PID) controller was activated from Posture 1 to Posture 2, as shown in Fig. 15(a).

In Experiment 2, to measure the fingertip force of the robot finger, we connected the robot finger and a load cell through a connection wire, as shown in Fig. 15(b). To apply the same torque for both modes, the motor current was feedback-controlled by using a current sensor (WCS1702).

Note that the robot finger in Cases A and C moves purely in Mode I, while in Cases B and D, it moves only in Mode II.

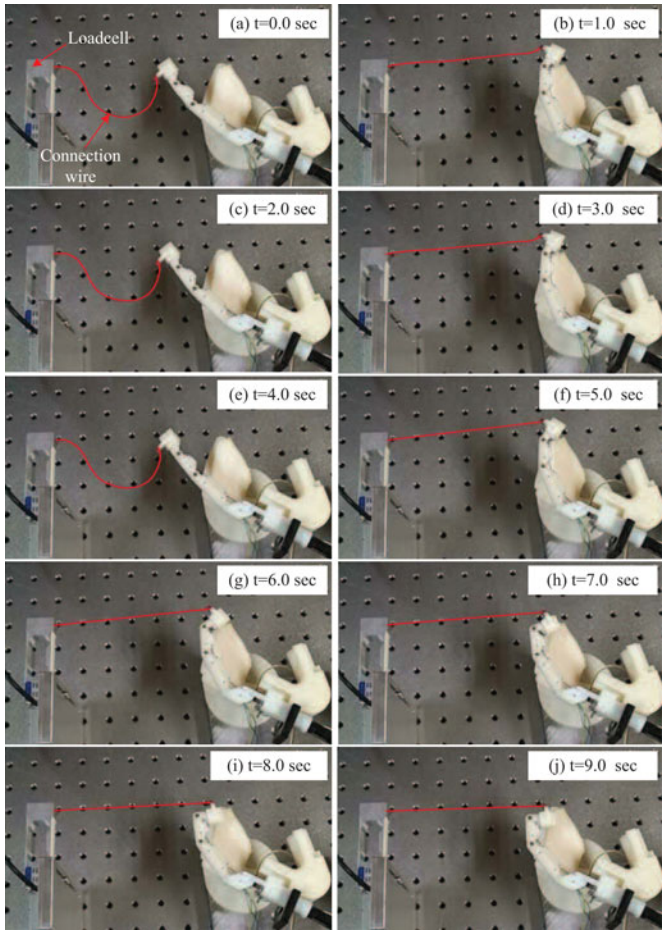

Fig. 13. Demonstration of a dual-mode robot finger. (a)–(e) Bending and extending motions repeated twice, and (f)–(j) forcing motion in Mode II.

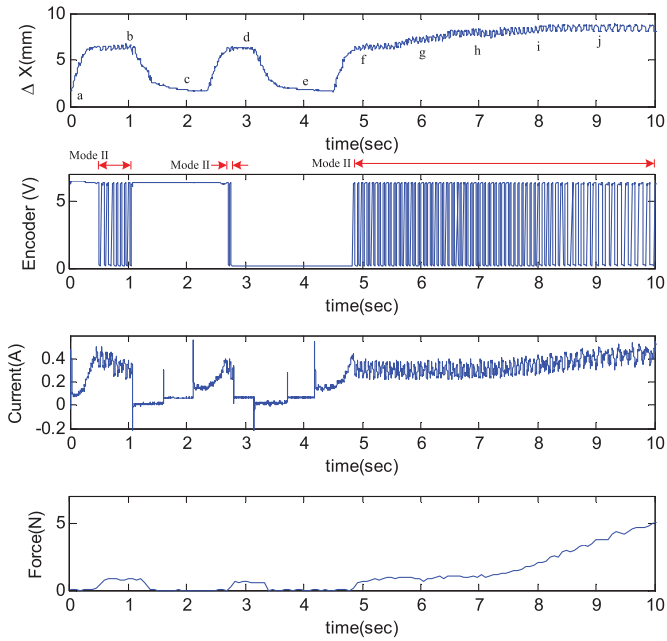

Fig. 14. Measured results for the operation of a dual-mode robot finger. The indication letters of a–j match to the subfigures in Fig. 13.

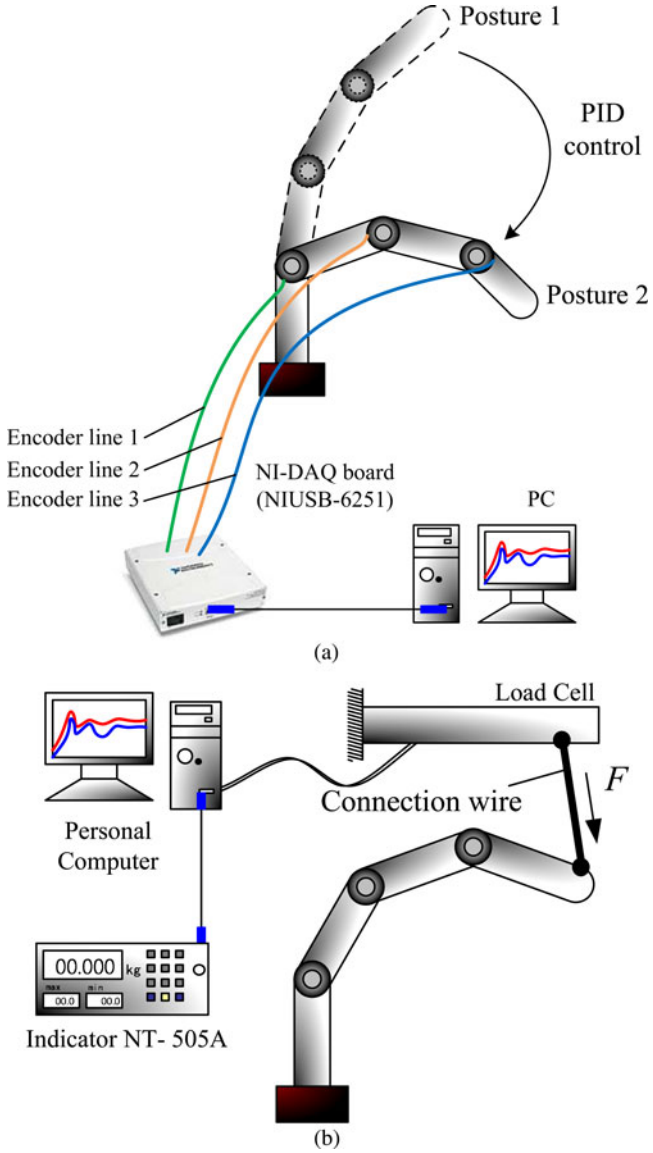

Fig. 15. Experimental setup used for performance measurements. (a) Measurement of the bending motion speed. (b) Measurement of the fingertip force.

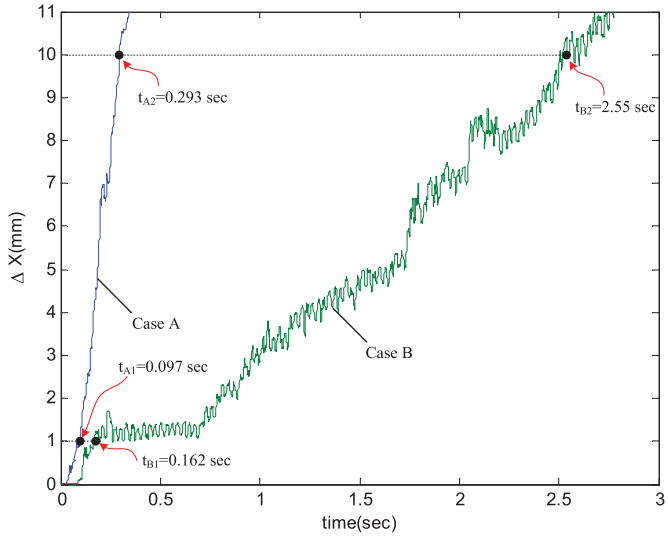

Fig. 16. Experimental results for measuring the motion speeds.

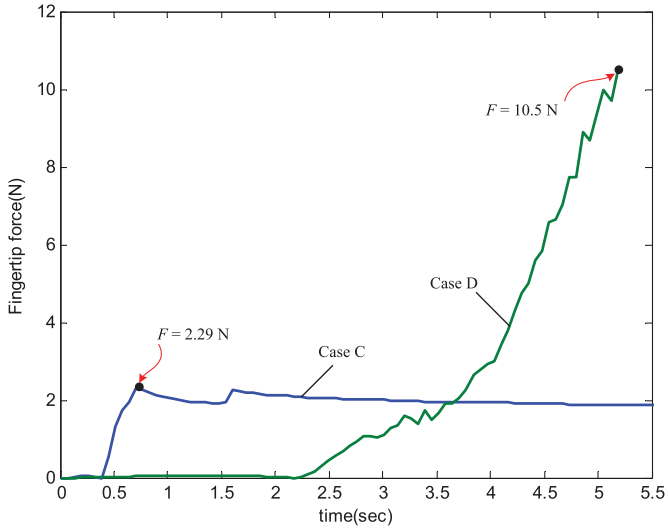

Fig. 17. Experimental results for measuring the fingertip forces.

TABLE III
EXPERIMENTAL CONDITION FOR FOUR CASES

Experiment 1: Measurement of bending speed	Items	Case A	Case B
	Friction	$\tau_b > \tau_m$	$\tau_b = 0$
	Motor Speed	9000 rpm	9000 rpm
Experiment 2: Measurement of fingertip force	Items	Case C	Case D
	Friction	$\tau_b > \tau_m$	$\tau_b = 0$
	Current	0.4 A	0.4 A

The experimental data were obtained through a data-acquisition board (NI-USB6251, National Instruments Corporation, Austin, TX) and a load cell indicator (NT-505A, CAS Corporation, Republic of Korea).

B. Discussion

For each of the cases, the experimental results are shown in Figs. 16 and 17. From Posture 1 to 2, in Experiment 1, the average contraction speeds are as follows:

$$\bar{V}_I = \frac{\Delta X_2 - \Delta X_1}{t_{A2} - t_{A1}} = 45.7 \text{ mm/s, for Case A}$$

$$\bar{V}_{II} = \frac{\Delta X_2 - \Delta X_1}{t_{B2} - t_{B1}} = 3.77 \text{ mm/s, for Case B.}$$

In spite of the same rotation speed of the motor, the contraction speed in Case A is 12.1 times faster than that in Case B.

From Experiment 2, the maximum fingertip forces reach 2.29 N in Case C and 10.5 N in Case D. Despite the application of the same motor torque for both cases, the fingertip force in Case D is 4.61 times larger than that in Case C.

The experimental results are summarized in Table IV and compared with the simulation results.

The results show that the dual-mode twisting mechanism does provide a fast bending motion of the robot finger in Mode I and a large grasping force in Mode II using a single motor, which allows the compact design and high performances of the robotic devices.

TABLE IV
SUMMARY OF EXPERIMENTAL RESULTS

Items	Measured value	Simulated value	Error(%)
$\frac{\dot{V}_I}{\dot{V}_{II}}$	12.1	12.7	4.7
$\frac{F_{II}}{F_I}$	4.61	4.88	5.5

As a remark, for the simulation of F_{II}/F_I in Table IV, the value of $\tau_f = 0.009$ N·m is adopted, which was obtained not arbitrarily but by a numerical fitting process based on the experimental data due to the difficulty in the direct measurement of the friction. Note that the numerical fitting process sweeping the allowable values of τ_f achieves the simulated value of F_{II}/F_I, which is close to the measured value. Considering that $\tau_m = 0.02$ N·m, the generated contraction force was decreased to 45% of the nonfrictional case (i.e., $\tau_f = 0$). This implies that the friction is a major factor, in practice, to degradation of performance. Lubrication and the usage of bearings at the contact points should be considered to enhance the design.

VI. CONCLUSION

In this paper, we newly presented a dual-mode robot finger that simultaneously achieves fast bending motion and a large grasping force with a single motor. By embedding a dual-mode twisting mechanism, the robot finger moves fast in Mode I, and can generate a large grasping force in Mode II. To demonstrate the effectiveness of the proposed method, we developed a dual-mode robot finger with a single DC motor that weighs only 29.9 g. The simulation and experimental results verified the notable performance enhancement of the proposed dual-mode robot finger, which provides a motion 12.1 times faster and a fingertip force 4.61 times larger, depending on the operation modes. The proposed mechanism is expected to be effectively adopted for the robot hand design with light weight and a small number of motors.

Future work will focus on precision grasping, the feedback control strategy, and the natural relaxation motion.

ACKNOWLEDGMENT

The authors would like to express their gratitude to Prof. K.-H. Rew for his keen insight and advice. They would also like to acknowledge the valuable and constructive comments provided by the anonymous reviewers.

REFERENCES

[1] Y. J. Shin and K.-S. Kim, "Distributed actuation mechanism for a finger-type manipulator: Theory and experiments," *IEEE Trans. Robot.*, vol. 26, no. 3, pp. 569–575, Jun. 2010.

[2] H. Liu, P. Meusel, N. Seitz, B. Willberg, G. Hirzinger, M. H. Jin, Y. W. Liu, R. Wei, and Z. W. Xie, "The modular multisensory DLR-HIT-Hand," *Mech. Mach. Theory*, vol. 42, no. 5, pp. 612–625, 2007.

[3] T. Mouri, H. Kawasaki, and K. Umebayashi, "Developments of new anthropomorphic robot hand and its master slave system," in *Proc. IEEE/RSJ Int. Conf. Int. Robots Syst.*, 2005, pp. 3225–3230.

[4] C. Cipriani, M. Controzzi, and M. C. Carrozza, "Progress towards the development of the SmartHand transradial prosthesis," in *Proc. IEEE 11th Int. Conf. Rehabil. Robot.*, 2009, pp. 682–687.

[5] T. Maeno and T. Hino, "Miniature five-fingered robot hand driven by shape memory alloy actuators," in *Proc. 12th IASTED Int. Conf. Robot. Appl.*, 2006, pp. 174–179.

[6] V. Bundhoo, E. Haslam, B. Birch, and E. J. Park, "A shape memory alloy-based tendon-driven actuation system for biomimetic artificial fingers—I: Design and evaluation," *Robotica*, vol. 27, no. 1, pp. 131–146. 2009.

[7] I. Yamano and T. Maeno, "Five-fingered robot hand using ultrasonic motors and elastic elements," in *Proc. IEEE Int. Conf. Robot. Autom.*, Apr. 2005, pp. 2673–2678.

[8] A. Kargov, C. Pylatiuk, H. Klosek, R. Oberle, and S. Schulz, "Modularly designed lightweight anthropomorphic robot hand," in *Proc. IEEE Int. Conf. Multisens. Fus. Integr. Intell. Syst.*, Sep. 2006, pp. 155–159.

[9] N. Tsujiuchi, T. Koizumi, S. Nishino, H. Komatsubara, T. Kudawara, and M. Hirano, "Development of pneumatic robot hand and construction of master-slave system," *J. Syst. Des. Dyn.*, vol. 2, no. 6, pp. 1306–1315, 2008.

[10] N. H. Chuc, J. K. Park, N. H. L. Vuong, D. Kim, J. C. Koo, Y. Lee, J.-D. Nam, and H. R. Choi, "Multi-jointed robot finger driven by artificial muscle actuator," in *Proc. IEEE Int. Conf. Robot. Autom.*, May 2009, pp. 587–592.

[11] H. Liu, K. Wu, P. Meusel, G. Hirzinger, M. H. Jin, Y. W. Liu, S. W. Fan, T. Lan, and Z. P. Chen, "A dexterous humanoid five-fingered robotic hand," in *Proc. 17th IEEE Int. Symp. Robot Human Interact. Commun.*, Aug. 2008, pp. 371–376.

[12] M. C. Carrozza, G. Cappiello, G. Stellin, F. Zaccone, F. Vecchi, S. Micera, and P. Dario, "A cosmetic prosthetic hand with tendon driven under-actuated mechanism and compliant joints: Ongoing research and preliminary results," in *Proc. IEEE Int. Conf. Robot. Autom.*, Apr. 2005, pp. 2661–2666.

[13] C. Cipriani and M. Controzzi, "Embedded hardware architecture based on microcontrollers for the action and perception of a transradial prosthesis," in *Proc. 2nd Biennial IEEE/RAS-EMBS Int. Conf. Biomed. Robot. Biomechatron.*, Oct. 2008, pp. 848–853.

[14] T. Takaki and T. Omata, "Grasp force magnifying mechanism for parallel jaw grippers," in *Proc. IEEE Int. Conf. Robot. Autom.*, Apr. 2007, pp. 199–204.

[15] T. Takaki and T. Omata, "High-performance anthropomorphic robot hand with grasping-force-magnification mechanism," *IEEE/ASME Trans. Mechatronics*, vol. 16, no. 3, pp. 583–591, Jun. 2011.

[16] T. Takayama, T. Yamana, and T. Omata, "Three-fingered eight-DOF hand that exerts 100-N grasping force with force-magnification drive," *IEEE/ASME Trans. Mechatronics*, vol. 17, no. 2, pp. 218–227, Apr. 2012.

[17] T. Wurtz, C. May, B. Holz, C. Natale, G. Palli, and C. Melchiorri, "The twisted string actuation system: Modeling and control," in *Proc. IEEE/ASME Int. Conf. Adv. Intell. Mechatron.*, Jul. 2010, pp. 1215–1220.

[18] T. Sonoda and I. Godler, "Multi-fingered robotic hand employing strings transmission named 'Twist Drive,'" in *Proc. IEEE/RSJ Int. Conf. Intell. Robots Syst.*, Oct. 2010, pp. 2733–2738.

[19] M. Suzuki and A. Ichikawa, "Toward springy robot walk using strand-muscle actuators," in *Proc. 7th Int. Conf. Climb. Walk. Robots*, 2004, pp. 467–474.

[20] J. L. Fu and N. S. Pollard, "On the importance of asymmetries in grasp quality metrics for tendon driven hands," in *Proc. Int. Conf. Intell. Robots Syst.*, 2006, pp. 1068–1075.